Results in Engineering 25 (2025) 103955

Contents lists available at ScienceDirect

Results in Engineering

journal homepage: www.sciencedirect.com/journal/results-in-engineering

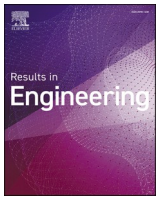

Unveiling the startup characteristics of pump as turbine using computational and experimental techniques

Dessie Tarekegn Bantelay [a,*], Girma Gebresenbet [a,b], Bimrew Tamrat Admasu [a], Muluken Temesgen Tigabu [a], Muluken Zegey Getie [a]

[a] Faculty of Mechanical & Industrial Engineering, Bahir Dar Institute of Technology, Bahir Dar University, P.O.Box 26, Ethiopia
[b] Department of Energy and Technology, Swedish University of Agric Sciences, SLU, Box 7032, Uppsala 750 07, Sweden

ARTICLE INFO

Keywords:
Startup characteristics
Transient characteristics
Pumps as turbines
Computational fluid dynamics (CFD)
Unsteady flow

ABSTRACT

Over time, the interest in using pumps as turbines (PATs) instead of conventional turbines has increased. The nature and operation challenges of hydraulic resources necessitate frequent starts and stops, resulting in severe fluctuations caused by fluid flow that led to machine deterioration. Gaining more insight into how the flow develops during transients allows for safe operating conditions, effective production planning, and estimating the cost variation due to operational changes. Currently, there are limited studies on the properties of pumps that function as turbines (PATs) at startup. This work analyzes the PAT's transient behavior over time while the system is starting up. A test rig was constructed for the centrifugal PAT to reveal its transient characteristics during the start-up process. In addition to the experiments, flow-dynamic simulations were run using ANSYS-Fluent. The rotating part's angular velocity was validated against experimental data. Transient characteristics such as the flow rate, head, torque, and tangential force of the PAT, etc., as well as the internal flow during the start-up, were analyzed. During the start-up transient phase, the transient characteristic parameters such as pump rotational speed, head, and flow rate change significantly. As the rotating speed approaches the rated speed, there is an increase in the transient impact head to a peak that is 2.04 times that of the rated head. The numerical simulation's outcomes and the experimental data were in excellent agreement.

1. Introduction

Effective energy conversion and utilization continue to be a growth-inhibiting factor in developing countries [1]. Pumps as turbines (PAT) for small-scale hydropower, pressure relief valves, and hydro-pumping applications have recently gained popularity [2]. Pumps as turbines (PAT) have developed into a viable and affordable energy-producing option. Researchers have been exploring various techniques to enhance the efficiency and applicability of PAT. This includes challenges and prospects [3], developing the best efficient point prediction model [4–7], enhancing efficiency [8], creating control systems [9], and mitigating cavitation [10–12]. Current research on pumps as turbines primarily focuses on developing PAT performance prediction methods under steady-state conditions [7,13–16]. On the other hand, research on the analysis of the transient behaviors of PAT systems during startup, shutdown, and load changes has gained less attention [17]. The PAT startup transition process can have a significant impact on the performance and reliability of the device. A seamless start-up can improve the reliability and efficiency of power systems [18]. During the PAT startup process, performance factors like pressure, flow rate, and rotating speed fluctuate quickly and significantly. This pushes the fluid flow into an unstable, momentary flow state that can quickly result in extremely high-pressure fluctuations and shocks [14]. This leads to vibration and fatigue. It ultimately harms the apparatus and jeopardizes its reliable and secure functioning. This emphasizes the importance of predicting and preventing PAT damage during start-up, as well as increasing equipment utilization by ensuring an efficient and effective schedule at all levels of maintenance management, production management, and quality control tasks [19].

Theoretical, computational, and experimental studies have been conducted to investigate the transient characteristics and unsteady conditions of centrifugal pump operation [16,20–25]. Scholars have tackled issues related to steady-state performance prediction, pressure surges, water hammers, flow instabilities, and sudden pressure changes

* Corresponding author.
E-mail address: dessie.Tarekegn@bdu.edu.et (D.T. Bantelay).

https://doi.org/10.1016/j.rineng.2025.103955
Received 25 October 2024; Received in revised form 5 December 2024; Accepted 3 January 2025
Available online 4 January 2025

in an endeavor to recognize and mitigate possible hazards. To mitigate these transient phenomena, researchers explore various methods, including system design, valve selection, and surge protection measures. Studies on the transient characteristics of the pump revealed that it accelerates rapidly during the startup stage [26]. Research indicates that the outcomes of erratic forecasts were more trustworthy. Regrettably, the pump's inversion design prevents the pump characteristic from indicating the turbine mode of operation. As a result, researchers have shown a keen interest in exploring the startup characteristics of pumps operating as turbines. Y.L. Zhang et al. [27] conducted a theoretical and experimental investigation on the transient properties of a PAT. Zhang & Zhao [28] used an experimental study to examine the PAT's transient performance during atypical startup process. An experimental investigation was carried out by Zhang et al. to determine how flow rate and rotational speed affect a pump's turbine startup characteristics [29]. Zhang et al. [5] additionally look into the theoretical model for forecasting how well pumps will operate as turbines at starting. In their start-up process, Chai et al. [30] conducted a computational study on the pressure fluctuation characteristics analysis of a centrifugal pump as a turbine. They found that the rise of flow rate and outlet static pressure exhibited shock phenomena, and the transient pressure fluctuation resulted in a distinction between the steady and dynamic features. Similarly, an experimental study showed that the transient period goes against the system curve to a significant amount [5]. Their studies usually center on the rotational dynamics and inertia of pump components during startup, as well as the establishment of hydraulic conditions. An investigation by Zhang et al. concentrated on strategies for controlling the flow rate and head during the acceleration phase [31].

In general, when a rotating machine, such as a pump as turbine, is connected to a fluid-filled system, the added mass effect occurs, increasing effective inertia [32]. A PAT reverses the pump impeller, allowing the flowing fluid to drive the impeller and generate power. During the PAT startup acceleration state, the added mass effect is particularly imperative. Literature has revealed that even though the added mass effect is substantial, other factors also influence the startup acceleration of a pump as a turbine [12]. These may include system characteristics, impeller design, and control strategies. According to their findings, the rotational speed of a PAT significantly influences its startup property. The torque requirements, acceleration rate, hydraulic transients, system response, and mechanical stresses all depend on the chosen rotational speed [29]. During startup, the rotational speed determines the torque needed to initiate and accelerate the impeller's rotation. In general, to overcome initial static friction and impeller inertia, high rotational speed and torque were required. In addition, the impeller's rotational speed affects the acceleration rate. Higher rotational speeds increase kinetic energy and lead to faster acceleration [31]. However, high startup acceleration may cause high mechanical stresses and hydraulic transients. This implies that understanding the startup phenomenon is crucial to controlling the startup acceleration within safe limits, and using appropriate control strategies like soft-start mechanisms or variable-frequency drives can help achieve a smooth and controlled startup process. In addition, the operating conditions, including the initial fluid flow rate and pressure, can influence the startup characteristics. Higher flow rates or pressures may necessitate more torque to accelerate the pump to its operational speed as a turbine.

In summary, key technical challenges associated with the pump as turbine start-up process including ensuring that the pump operating as a turbine start up is matched correctly to the specific operating conditions and requirements of the system including flow rate, head, speed, and efficiency; implementing control systems that are capable of effectively regulating the operation of the pump as a turbine; making necessary mechanical adaptations to enable it to function as a turbine involve modifications to bearings, seals, shafts, and other components to ensure reliable and efficient operation; and ensuring that the system is designed and operated in a manner that prioritizes safety and mitigates risks such as overspeed, mechanical failure, and hydraulic issues is essential. Addressing all performance matching, selecting and implementing appropriate control systems and mechanical adaptations, and ensuring safety concerns associated with operating a pump as a turbine is crucial and needs a detailed understanding of the startup process. More research is needed to improve the accuracy and reliability of PAT's transient behavior during startup. Different factors enter the depiction here, including inertia, added mass, and rotational speed. This was done using advanced numerical simulations and experimental validation. This will help us understand startup characteristics that were important for making the system work better, keeping equipment safe, and improving performance. Most current research on pumps and turbines focuses on performance relations and prediction under steady-state conditions, abandoning the fleeting aspects of the startup phase largely untouched. Based on these findings, the principal purpose of this paper is to offer further understanding of the transient phenomena of the PAT at starting using computational fluid dynamics (CFD). A 3-D simulation of PAT's transient start-up was used to reveal the effects of inertia, flow rate, and mass. This paper describes the computational fluid dynamic techniques and experimental setup in Section 2; the CFD and experimental outcomes were discussed and offered in Section 3, and the study result is summarized in Section 4.

2. Materials and methods

2.1. Analytical method

2.1.1. Characterization

The angular speed of the PAT distinguishes its startup process. In this regard, the PAT's angular speed passively increases throughout the startup process, and the CFD simulation typically obtains the relationship between starting torque and time variation to simulate start-up velocity. The power output of the PAT, neglecting friction power losses, is defined as:

$$M\omega = \rho g H Q \eta \tag{1}$$

The fluid flow torque, which causes the PAT impeller to rotate and accelerate linearly, defines the angular momentum as follows [29]:

$$M = J\frac{d\omega}{dt} \tag{2}$$

After rearranging Eq. (2), the angular speed was determined [33] as follows:

$$\omega_{i+1} = \omega_i + \frac{\mathrm{M}}{J}(t_{i+1} - t_i) \tag{3}$$

The PAT impeller's steady-state torque is comparative to the square of the pump speed. The analytical solution of the PATs' angular momentum across startup without any controlling mechanism is comparative to the square of the rotational speed of the PAT impeller. Eq. (4) [33] also allows for the determination of the angular speed.

$$\omega(t) = \omega_0 \tanh\left(\frac{C\omega_0}{J}t\right) \tag{4}$$

Where ρ is density of the medium in kg/m^3, g is gravitational acceleration in m s^{-12}, Q is the flow rate in m^3/s, H is pressure head in m, η is the PAT efficiency, M is the resultant torque in N.m, J is the rotational inertia of the impeller in kg.m^2, ω is the rotational speed in rad s^{-1}, ω_0 is the steady state speed, and C is a constant of proportion. At the early stage of startup, $t = 0$ and $\omega = 0$ are considered through the analysis.

2.1.2. Effect of flow rate

The effect of flow rate on the starting performance of a PAT was examined, starting at a low flow rate and gradually increasing to the highest range of flow rates. The important flow parameters, such as efficiency, pressure, torque, and power output, were analyzed during the startup process. The PAT is simulated at 0.5 Q_{BEP}, Q_{BEP}, and 1.5 Q_{BEP} at a

constant moment of inertia of 0.0198 kgm^2 and mass of 1.84 kg, where Q_{BEP} refers to the flow rate at the "Best Efficiency Point" at which the PAT operates with maximum efficiency.

2.1.3. Effect of impeller density

The moment of inertia of a pump as a turbine is its resistance to deviations in angular speed as it rotates about its impeller. Information of the moment of inertia of a PAT impeller is typically required for transient analysis of a PAT. The effect of the moment of inertia investigated kept the shape and size of the stationary blades, only altering the density of the blades by varying the material type. Using SolidWorks, a CAD pump model was created to determine the inertia at the specified density. Various blade densities were taken into account, as Table 1 illustrates, along with the materials used in the pump impeller. A reference case has been determined to be the middle value of $J = 0.1285$ kg/m^2 at the constant flow rate of Q_{BEP}. The parameter $J\ /Jref$ was employed to establish the influence of blade density on the PAT's initial performance.

2.1.4. Effect of added mass

As the fluid flows through the pump passages, the fluid's mass interacts with the pump's impeller as it begins to rotate. The fluid passing through the pump passage exerts a tangential force (*Ft.*) on the impeller blades, resulting in added mass effects. The added mass essentially increases the effective mass of the system, influencing both the rotational speed and the torque. At every incremental time interval, the CFD solver performs calculations to determine the tangential hydrodynamic force acting on the impeller blade. The accurate computation of the tangential force is essential for understanding how the impeller blade interacts with the fluid and enabling a detailed analysis of the additional mass. Therefore, by continuously assessing and incorporating the tangential hydrodynamic force at each time step, the CFD solver can effectively capture the dynamic impact of added mass, facilitating a more comprehensive understanding of the system's response and performance characteristics under different circumstances. A simplified expression is used to estimate the added mass, due to the complex nature of the velocity field. When the center of mass of a PAT is located at radius (R), the tangential acceleration is given by $dV/dt = Ra$, where $dV\ /dt$ represents the change of tangential velocity. Since the impeller radius remains constant regardless of the density, the tangential force exerted by the liquid flow on the impeller blade is altered by a change of added mass and tangential velocity, calculated as [34]:

$$F_t = (m_a + m_t)R\alpha \tag{5}$$

Substituting angular acceleration $\alpha = \mathbf{M}/J$ and rearranging Eq. (5). Added mass is calculated as:

$$m_a = \frac{J\,F_t}{M\,R} - \ m_t \tag{6}$$

Where F_t is the tangential force in N, m_a is fluid added mass in kg, m_t is mass of impeller in kg, R is impeller radius in m, V is impeller tangential velocity in m s^{-1}, and α is angular acceleration in rad s^{-12}.

To investigate the effect of blade density, flow rate, and added mass upshot on the startup acceleration of the pump as a turbine, seven independent simulations were carried out as presented in Table 2.

Table 1
The values of the model's impeller mass (m_t) and inertia (J).

Material type	ρ (kg/m^3)	m (kg)	J (kgm^2)	$J/Jref$ (-)
Brass	8500	16.6953	0.1517	1.1869
Bronze (commercial)	8800	17.2845	0.0230	1.1616
Grey cast iron	7300	14.1419	0.1285	1.00
Aluminum (1060)	2700	5.3032	0.0482	0.3737
Wood	159.9	0.3142	0.0029	0.0222

2.2. Computational method

Computational fluid dynamics is vital for accurate and rapid start-up performance prediction of fluid flow phenomena inside the PAT. ANSYS Fluent is a commercially available CFD tool that simulates and analyzes PAT flow behavior and performance characteristics during the startup process. This helps to achieve a full understanding of the fluid dynamics within PAT systems for better design and performance optimization. In addition, it provides detailed insights into complex fluid flow phenomena, empowering researchers to make up-to-date decisions and increase the PAT systems' efficiency.

2.2.1. Physical model

The single-stage horizontal centrifugal pump under study has a volute casing. In its construction, the model comprises essential elements like an impeller with six blades, inlet and outlet pipe extensions, volute casing, shroud, and hub. During PAT operation, the fluid flow is reversed; entering the outlet pipe directs the fluid flow towards the volute casing impeller, ensuring a consistent and controlled intake. Then, volute casing collects the fluid exiting the outlet pipe and converts its pressure energy into kinetic energy and directs it to the impeller. Then, impellers convert the kinetic energy of the fluid into mechanical energy. Finally, the inlet pipe carries the fluid away from the impeller after energy conversion. The shroud surrounds the impeller blades, providing structural support and directing the flow of fluid. The hub connects the impeller to the shaft, allowing for the transfer of rotational energy. Three-dimensional computational fluid dynamics models that simulate the fluid domains of the entire machine appropriate for transient numerical simulation were used [35]. The computational domain shown in Fig. 1 was generated using BladeGen, SolidWorks, and CATIA in combination to maintain surface integrity and geometry accuracy. Table 3 displays the principal design parameters of the PAT.

2.2.2. Governing equations and turbulence models

Multiple governing equations typically describe the fluid flow and energy conversion processes in PAT [36–48]. Generally, CFD solves incompressible turbulent flow using the continuity equation and the Reynolds-average Navier stock equation. The present study simulated the pump's internal flow during the start-up process using a 3D incompressible, transient, turbulent flow at a steady temperature. Consequently, the mass conservation equation is expressed as follows:

$$\nabla \cdot u = 0 \tag{7}$$

Furthermore, the momentum equation can be represented as follows:

$$\frac{\partial u}{\partial t} + u \cdot \nabla u = -\frac{1}{\rho}\nabla p + \nu \nabla^2 u \tag{8}$$

In this study, the widely used k-omega (k-ω) turbulence model is utilized [36,38–41,44]. This widely used two-equation turbulence model in PAT computation is an approximation of the Reynolds-averaged Navier-Stokes (RANS) equations. The two scalar turbulent kinetic energies, k and ω, of transport equations were solved using the K-ω turbulence model. The K-ω turbulence model offers plunders over the K-ε model when handling shear flow, boundary layer turbulence, and moderate separation turbulence [36]. The variable k represents the turbulence kinetic energy, while ω represents the specific rate of dissipation, indicating the conversion of turbulence kinetic energy (k) into internal thermal energy, as solved by Eqs. (8) and (9) respectively:

$$\frac{\partial(\rho k)}{\partial t} + \frac{\partial(\rho k u_i)}{\partial x_i} = \frac{\partial}{\partial x_j}\left[\left(\mu + \frac{\mu_t}{\sigma_k}\right)\frac{\partial k}{\partial x_j}\right] + G_k - \beta^* \rho \mathbf{k}\omega \tag{9}$$

$$\frac{\partial(\rho \varepsilon)}{\partial t} + \frac{\partial(\rho \varepsilon u_i)}{\partial x_i} = \frac{\partial}{\partial x_j}\left[\left(\mu + \frac{\mu_t}{\sigma_t}\right)\frac{\partial \varepsilon}{\partial x_j}\right] + \alpha\frac{\omega}{k}G_k - \beta\rho\omega^2 \tag{10}$$

Table 2
CFD simulation cases used in the study.

Case	Blade materials			Expected steady state flow rates			Fluid type		
	Brass	Cast iron	Aluminum	$0.5Q_{BEP}$	Q_{BEP}	$1.5Q_{BEP}$	air	water	oil
1		x		x				x	
2		x			x			x	
3		x				x		x	
4	x				x			x	
5			x		x			x	
6		x			x		x		
7		x			x				x

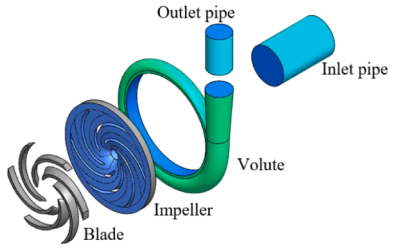

Fig. 1. 3D geometry of the pump as turbine.

Table 3
Main design parameters of the pump as turbine.

Nominal Parameters	Symbol	Value
Design flow rate [m^3/s]	Q_e	*0.03*
Design head [m]	H_e	*25.5*
Rotational velocity [RPM]	N	*1450*
Motor power [kW]	P_e	*10.7*
Specific speed [-]	N_s	*1179*
Number of vans [no]	Z	*6*

Where G_k is the generation term of turbulence and μ_t is the relationship between the turbulence frequency and viscosity, solved by Eqs. (10) and (11) respectively:

$$G_k = \mu_t \left(\frac{\partial u_i}{\partial x_j} + \frac{\partial u_j}{\partial x_i} \right) \frac{\partial u_i}{\partial x_j} \tag{11}$$

$$\mu_t = \rho \frac{\mathbf{k}}{\omega} \tag{12}$$

Moreover, the study employs Bernoulli's equation, which describes the head of the pump operating as a turbine as follows:

$$H = \frac{p_1 - p_2}{\rho g} + \frac{c_1^2 - c_2^2}{2g} + (z_1 - z_2) \tag{13}$$

Where p is static pressure in Pa, z is position head in m, and c is absolute velocity in m s^{-1}. The subscripts 1 and 2 denote the pump's inlet and outlet, respectively.

2.2.3. Mesh generation

Using the integrated ANSYS meshing module, we performed meshing after extracting the three-dimensional geometric flow domain. Researchers have experimented with different grid generation techniques for PAT CFD simulations. While some investigators utilized both structured and unstructured elements in combination, most researchers took advantage of unstructured tetrahedral elements [49]. This study utilized

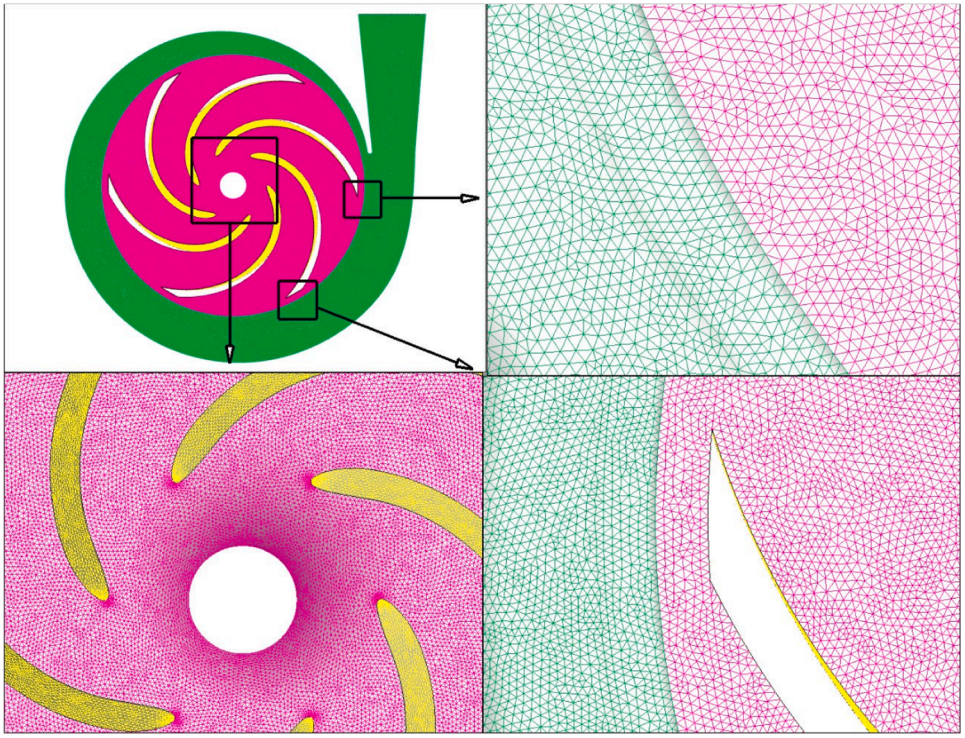

Fig. 2. Unstructured tetrahedral computational grid utilized in the flow domains of PAT.

unstructured tetrahedral grids. The tetrahedral mesh can provide more accurate calculation results [36]. Fig. 2 depicts the mesh refinement near the pump's critical zones, encompassing the blades' leading and trailing edges and the volute tongue. Mesh density and quality have a crucial role in achieving accurate CFD results. Then, it is necessary to have a high-density and high-quality grid to capture complex flow phenomena, such as flow separation and recirculation through flow passages. However, as the grid density increases, so do the computational time and computational facility requirements. As a result, a balance between grid quality and computational efficiency is crucial for conducting reliable and efficient simulations.

2.2.3.1. Grid size independence test. To validate that the CFD solution is insensitive to variations in grid size, a grid convergence study was performed. By increasing the number of elements gradually from 0.47 million to 12.30 million. For turbomachinery, efficiency is a critical parameter. It is therefore closely observed during these simulations. Using Eqs. (14)–(16).

$$P_{in} = Q(P_1 - P_2) \tag{14}$$

$$P_{out} = M\omega \tag{15}$$

$$\eta = \frac{P_{out}}{P_{in}} \tag{16}$$

Where P_2 *and* P_1 were the outlet and inlet total pressures, respectively. Q is the volume flow rate, ω is the angular velocity [50], and M is the total moment of the impeller.

Fig. 3 shows the computation outcomes with various grid numbers. The findings indicate that there was no significant change in the computed efficiency values between grid sizes of 7.18 and 12.30 million. Consequently, a grid with approximately 7.18 million elements was selected for further simulations to optimize computational costs.

2.2.3.2. Grid quality independence test. The Ansys-Fluent user manual provides a guideline for assessing grid quality using skewness values. Skewness refers to the distortion or non-orthogonality of grid elements. The histogram in Fig. 4 shows the frequency distribution of the skewness of the elements that correspond to the present study. In this study, 12.9 % of elements have 0.05, 31.4 % have 0.15, 33.4 % have 0.25, and 19 % have 0.35 skewness. In addition, only 1 % of the elements were above 0.5 skewness. The maximum reported skewness in this study is 0.85, affecting only insignificant numbers of elements (0.0001 %). The highly skewed elements were few and far away from the region of interest; as a result, their effect on the computational results is insignificant.

2.2.3.3. Time-step independence test. To ensure that the CFD solution remained unchanged due to time step length difference, a time-step independence test was performed using the time-step sensitivity study method. It involves running the simulation with varying time steps while keeping the remaining simulation parameters unchanged. This study evaluated four-time steps: t = 0.0001 s, 0.0005 s, 0.001 s, and 0.0015 s, using the ANSYS fluent guide. The mass flow rate was monitored at 36 kg s^{-1}, and J is equal to 0.02 kgm^2. A comparison of the simulation's output is displayed in Fig. 5. The analysis indicates that a time step of $\Delta t = 0.001$ s was appropriate for all subsequent simulations in this study.

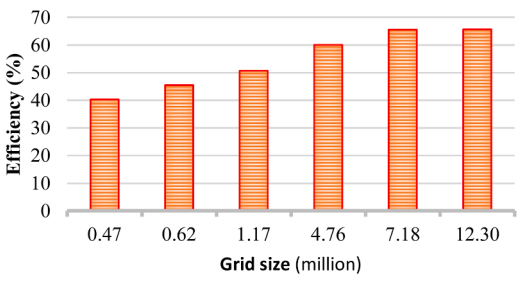

Fig. 3. Computational grid independence test result.

2.2.4. Boundary conditions

Cell zones represent solid and fluid regions in CFD simulations, while face zones represent internal surfaces and boundaries. Assigning appropriate boundary conditions to face zones is critical to ensuring meaningful values for each variable equation and accurate results across the entire domain. The study treats the casing as a stationary reference frame and the impeller as a rotating reference frame. To achieve accurate results, coupled pressure-velocity coupling methods were employed, such as the Green-Gauss node-based gradient. In addition, pressure, momentum, kinetic energy, and dissipation rate were computed using second-order techniques. A frozen-rotor interface model determines the coupling between the stationary casing and the rotating impeller. This model creates an interface connecting the impeller and casing, enabling the sharing of relevant flow data. The walls associated with the impeller were designated as rotating, while the walls associated with the casing were designated as stationary. Non-slip boundary conditions were applied to the impeller blades and casing walls to ensure realistic flow behavior. These conditions assume that the fluid in direct contact with these surfaces adheres to them without slipping. Table 4 summarizes the boundary conditions employed by various researchers in the computational studies of pumps as turbines. The pressure and volume flow rate boundary conditions at the PAT inlet and outlet were used interchangeably by researchers. Table 4 presents a summary of the boundary conditions used in previous studies, facilitating comparison and understanding of the choices made in the present study. Overall, the selection and accurate definition of appropriate boundary conditions were crucial for generating reliable results in computational studies of centrifugal pumps.

To validate the CFD setup, a constant mass flow rate of 30 kg s^{-1} for the pump as a turbine (PAT) inlet, along with a 5 % turbulence intensity, was set. Similarly, the outlet boundary condition is specified as 1 bar total pressure. In addition, the walls of the PAT were modeled as solid walls to enforce a no-slip condition, ensuring that the fluid velocity at the walls remains zero. Interfaces between the inlet pipe and impeller and the impeller and volute casing were defined. These conditions facilitate proper fluid exchange between the components, allowing for the transfer of mass, momentum, and energy across the interface. The computational study aims to capture PAT behavior at different flow conditions.

The pressure and velocity were coupled using the SIMPLE technique. It integrates two algorithms for pressure correction: SIMPLE [51] and PISO [52], as, correspondingly, inner and outer corrective loops. At each time step, ten outer correction loops at most are performed according to a residual criterion. After four outer correction loops, the flow solution converges at most time steps. Each outer loop carries two inner correction loops. To ensure explicit term convergence, after every inner loop was performed, one extra non-orthogonal corrective loop. Furthermore, the turbulent flow was considered when utilizing the usual k-ω model. Table 5 presents a summary of the boundary conditions used in the study.

2.2.5. Dynamic mesh setting

The dynamic mesh feature allows for the simulation of moving or deforming boundaries. The transient operation of PAT was studied using the dynamic meshing technique. This involves two types of mesh motion at the same time: rigid body rotation of the impeller as a single body and mesh deformation resulting from the rotation of the impeller blades. The rigid body rotation function controls the rotations of the runners. The first PIMPLE outer correction loop updates the mesh at each time step. After that, the face fluxes were computed using the relative fluid velocity and face-swept volumes [53,54].

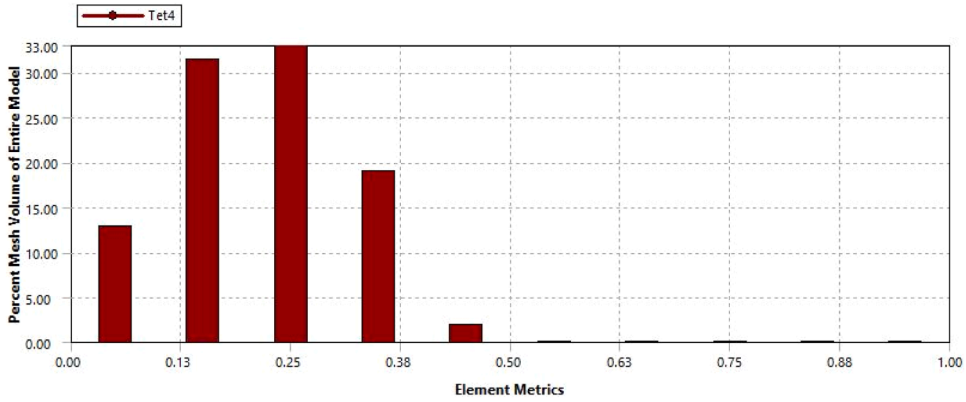

Fig. 4. Grid quality test as a function of number of elements versus skewness.

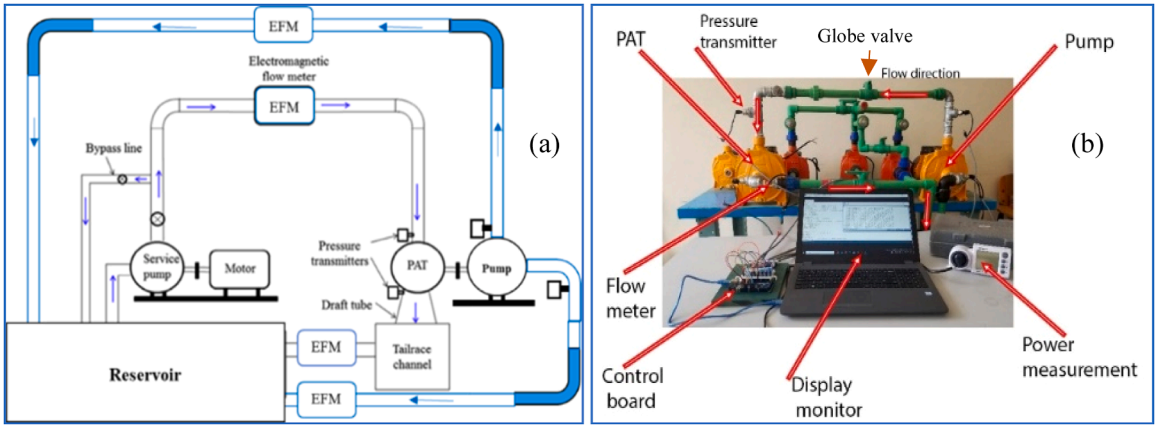

Fig. 5. A schematic drawing of the experimental setup used in the present study.

2.3. Experimental verification

Experiments were carried out in the Bahir Dar University thermos fluid laboratory to validate the numerical simulations. The test rig used in the present experimental study is shown in Fig. 5. The centrifugal pump is driven by a 2 kW electric motor with a maximum rotational speed of 1630 rpm. The pump is connected by pipe to a reservoir, making a closed loop, and the whole assembly is mounted on a base carrier. Flow rate regulation is made by throttling a globe valve installed on the discharge side of the pump. The valve located at the inlet of the pump is used in the study of the effect of low pressure on the performance of the pump as well as the formation of cavitation [55]. Suitable sensors were integrated into the system to allow an accurate analysis of pump performance. Two electronic pressure sensors were attached to the equipment, one at the pump inlet and the other at the pump outlet. The pump flow rate is measured using a rotary flowmeter. A temperature sensor is located at the tank outlet to measure the liquid temperature in the system. The pump operations were controlled by software on a suitable computer via an interface device. The software displays all sensor readings on the computer screen in tabular form.

2.4. Calibration of experimental setup

The calibration of the experimental setup was made by measuring flow rate and pressure using two different devices, as shown in Figs. 6 and 7. In this regard, the flow meter (better than 1 %) and pressure gauge (0.15 % FS) with known accuracy were used to calibrate the Arduino-based sensors developed in this work. The calibration procedure includes four different pressure and flow rate values for the setup that were tested. As shown in Fig. 6, the different flow rate values were measured using a clamp-on ultrasonic flow meter and the Arduino-based device. The clamp-on ultrasonic flow meter uses a V-method installation and comprises an electronic display/interface unit with built-in software, a data logger, a power supply (1), downstream transducers (2), and upstream transducers (3).

Likewise, the different pressure values were measured as shown in Fig. 7 using a digital pressure gauge (3) with a data logger and USB interface and the Arduino-based control board (2), signal transmitter cables (1), and pressure transducer (4). To measure flow rates, we use the JFA490 portable handheld pipeline clamp-on ultrasonic flowmeter, which is ideal for online liquid flow calibration and inspection. With an accuracy of better than 1 %, repeatedly better than 0.2 %, and a working power of 90~230 VAC Ni-MH rechargeable batteries, it can work for 10 h on a full charge. It is an external installation application with a four-line format for transient flow, speed, accumulated flow, and signal status. The non-isolated RS232 (FUJI Extended Agreement) signal output enables the internal data recorder to store data, and it utilizes specialized software to transfer data to computers. The high-speed sample rate used to record the pressures was up to 1 kHz on a computer using the UPS-HSR digital pressure sensor. It has a USB output signal, an accuracy of 0.15 % FS, electrical connections with a USB mini-B cable (5), process connections with a G1/4 or 1/4 NPT $\leq$ 1500 bar, and an AE F-250-C female $>$ 1500 bar It works with media that is made of titanium alloy and has special features like a sampling rate of up to 1000 Hz and a resolution of 21 bits $\leq$ 5 Hz or 16 bits $>$ 5 Hz.

The measured values were shown in Table 6. A maximum deviation of 0.9 % was recorded from the flow rate measurement. An average deviation of 0.41 and 0.39 % were used as a calibration factor for

Table 4
Review of PAT boundary conditions, turbulence model, and solver used in computational studies.

Authors	Year	Inlet	Outlet	Turbulence Model	Solver
X. Bai et al. [37]	2023	Velocity inlet	Static pressure	k–epsilon (*k–ε*)	–
Hu et al. [36]	2023	Mass flow	Static pressure	k–omega (*k–ω*)	Fluent
Y. Wei et al. [38]	2023	Pressure inlet	Pressure (1 atm)	k–omega (*k–ω*)	–
D. Jianguo et al. [39]	2020	Static pressure (1 atm)	Mass flow rate	k–omega (*k–ω*)	CFX
T. Lin et.al [40]	2021	Mass flow	Static pressure	k–omega (*k–ω*)	CFX
Li, Meng, & Qiao [41]	2020	Static pressure	mass flow rate	k–omega (*k–ω*)	CFX
D. Stefan et al. [42]	2020	Volumetric flow rate	Static pressure (1 bar)	–	CFX
M. Rossi, et al. [43]	2019	Volumetric flow rate	Static pressure (1 bar)	–	CFX
D. Adu et al. [44]	2019	Static pressure	Mass flow rate	k–omega (*k–ω*)	CFX
E Frosina et al. [45]	2017	Volumetric flow	Pressure	k–epsilon (*k–ε*)	–
M Pére z-Sánchez et al. [46]	2017	Static pressure	Volumetric flow rate	–	FloEFD
S.S. Yang et al. [47]	2012	Static pressure	Volumetric flow rate	k–epsilon (*k–ε*)	CFX
J Fernández et al. [48]	2010	Pressure (1 atm)	Mass flow rate	–	Fluent

Table 5
Conditions that served as study boundaries.

PAT Boundary	Boundary conditions
PAT inlet	Mass flow rate
PAT outlet	Total Pressure
Vans	Rotating wall
Impeller	Rotating wall
Volute casing	Stationary wall
Inlet Pipe	Stationary wall
Interface between inlet pipe and impeller	Fluid – fluid interface
Interface between casing and impeller	Fluid – fluid interface

pressure and flow rate, respectively, for the subsequent experimental measurements.

3. Results and discussions

3.1. Validation

The model PAT setup has been validated using the developed test bench. The test bench enables us to measure the rotational speed of the PAT at startup. Fig. 8 presents a comparison between the numerical and experimental results. The tendency of the PAT's numerically predicted performance curves corresponds to that predicted using the experiment. The numerically predicted results were higher than the experimental results. A maximum deviation of 9 % was recorded at start-up, and an average deviation of 2 % was recorded through 25-time interval measurements. Moreover, both the experimental and numerical data show a similar trend. The higher rotational speed of the CFD result may be attributed to the neglect of leakage and mechanical losses. The comparison between the numerical and experimental results shows that the numerical setups were appropriate for the PAT's startup performance analysis.

3.2. Transient simulation

A transient state simulation has been developed in order to evaluate the inertial behavior of the pump as a turbine in transient conditions. Figs. 9–11 show the instantaneous head, momentum, and force during the PAT start-up process. The figures illustrate how the machine gradually stabilizes after a sudden initial drop. During the startup of a pump operating as a turbine, as shown in Fig. 9, significant head variations occur as the fluid flow increases slowly, causing the impeller to rotate and the system to experience changes in momentum due to the accelerating fluid. This change in momentum affects the impeller's rotational speed and the torque it exerts on the shaft. Transient effects during startup, such as variation in head, momentum, and force, occur as the system transitions from rest to operating conditions, potentially impacting the performance and stability of the pump operating as a turbine. Throughout the simulation, significant variations in the head data were observed. The maximum fluctuation, reaching 61.6 %, was recorded at $t = 0.024$, indicating a moment of pronounced change in the system. This sharp peak was followed by an average steady-state variation of 8.2 %. Interestingly, as the simulation progressed, the minimum variation was documented at the end, underscoring the convergence towards a stable state. These observations highlight the dynamic nature of the system under study, showcasing both drastic shifts and gradual settling towards equilibrium as time elapsed. In addition, the effect of factors affecting pump performance, including thickness of the clearance at the shroud side, radial leakage into the inlet side, and change in fluid properties, was noticed [56].

Fig. 10 describes rotational behavior, which indicates an initial counterclockwise rotation of the machine for a short period before abruptly shifting to a clockwise direction, reaching a peak torque value of 50 N.m. Subsequently, the torque decreases and stabilizes at a lower value of 12 N.m. The torque fluctuation indicates unexpected pressure variations that could potentially harm the impeller blades. The rapid change in rotational direction and substantial torque peaks can put a lot of strain on the impeller blades. Such fluctuations in torque and direction can lead to uneven loading on the blades, causing them to experience varying levels of force and pressure. This uneven distribution of forces can result in localized stress concentrations on the blades, potentially leading to fatigue, deformation, or even failure over time. Exposure of the impeller blades to these unintended pressure increases

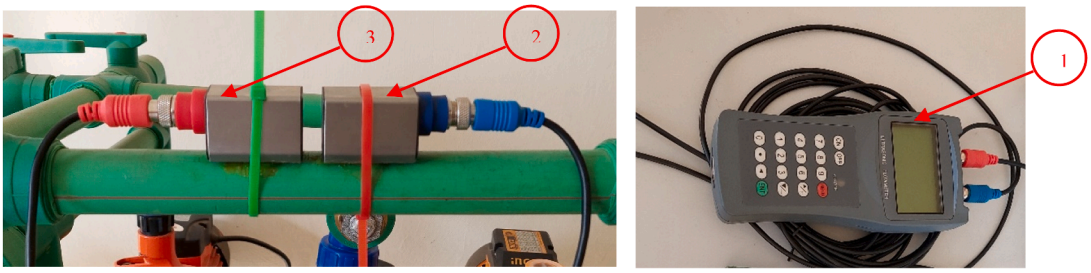

Fig. 6. Flow rate measurement calibration set up.

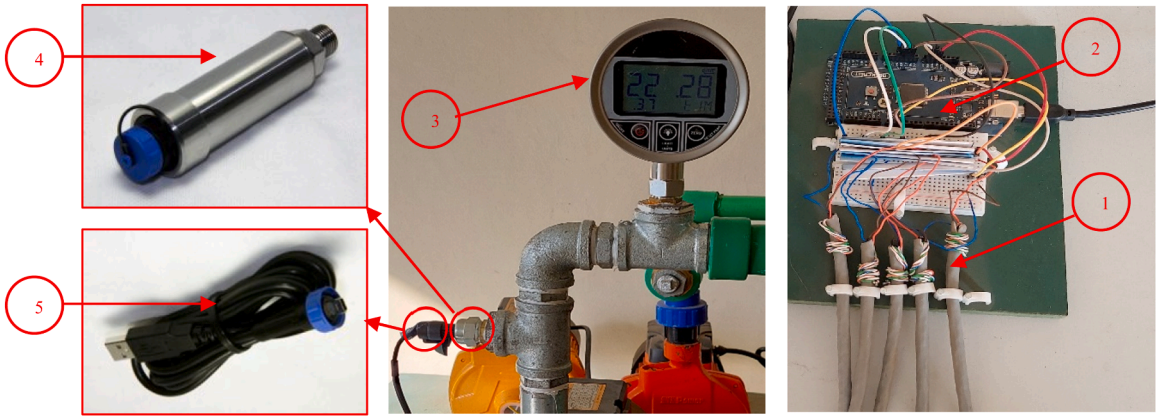

Fig. 7. Pressure measurement calibration set up.

Table 6
Summarized calibration result of Arduino-based flow meters and pressure sensors.

Test	Arduino-based inline flow meter (m^3)	Clamp-on ultrasonic flow meter (JFA490)	Arduino-based pressure sensor (Pa)	Digital pressure gauge (UPS-HSR)
1	179,316.00	177,881.50	0.014880	0.015
2	196,794.70	195,810.70	0.017910	0.018
3	255,484.90	253,696.50	0.023832	0.024
4	285,537.30	284,395.20	0.029880	0.030
5	328,982.80	327,995.90	0.035892	0.036
6	372,458.70	370,223.90	0.038766	0.039
7	406,357.80	405,951.40	0.041958	0.042
8	446,271.10	442,254.70	0.044595	0.045
9	487,430.00	486,942.60	0.047952	0.048
10	531,357.20	530,294.50	0.050898	0.051
11	576,101.40	574,373.10	0.053838	0.054
Average	369,644.72	368,165.40	0.036400	0.036

poses a significant risk to the components' structural integrity. The repeated exposure to such dynamic loading conditions can accelerate wear and tear, reducing the operational lifespan of the impeller and increasing the likelihood of premature failure. Therefore, it is critical to analyze and address these torque fluctuations to prevent damage to the impeller blades and ensure the machine's reliable and safe operation over its intended service life.

Similarly, Fig. 11 demonstrates the tangential force variations on the blade surface. When a pump functions as a turbine (PAT) and faces a tangential force exceeding three times its steady-state value, it can lead to severe implications affecting both performance and structural stability. The heightened force places considerable mechanical strain on crucial PAT components, notably the impeller and shaft, potentially causing fatigue, distortion, or structural breakdown if these elements were not engineered to endure such intense forces. Excessive tangential forces may trigger system vibrations, inducing operational instability and impacting overall performance by reducing efficiency, escalating wear and tear, and risking damage to various parts. This increased force can hasten wear on vital elements like bearings, seals, and the impeller itself, reducing the system's longevity, increasing maintenance requirements, and resulting in unforeseen downtime. The disruption caused by very high tangential forces can disturb fluid flow dynamics within the system, diminishing PAT efficiency and leading to elevated energy consumption, diminished performance, and reduced productivity. Operating a PAT under excessive tangential forces poses safety risks, potentially causing equipment damage, operational dangers, and endangering personnel nearby due to structural failures or component malfunctions. Prolonged exposure to tangential forces well above the steady-state value can inflict lasting harm on the PAT system, gradually compromising its reliability and necessitating costly repairs or replacements. In essence, subjecting a pump operating as a turbine to extremely high tangential forces can trigger significant outcomes, including mechanical stress, vibrations, wear, efficiency declines, safety hazards, and long-term damage. Vigilant monitoring and control of these forces within safe limits were imperative to uphold the optimal performance, durability, and safety of the PAT system.

3.3. *Pressure fluctuation*

The pressure fluctuation through time at the PAT's inlet during the startup process is presented in Fig. 12. The pressure variation magnitude is the principal at the start-up stage, which is 2.04 times the average steady state value. This may be attributed to sudden changes in flow, transient effects, impeller and blade effects, cavitation, and system

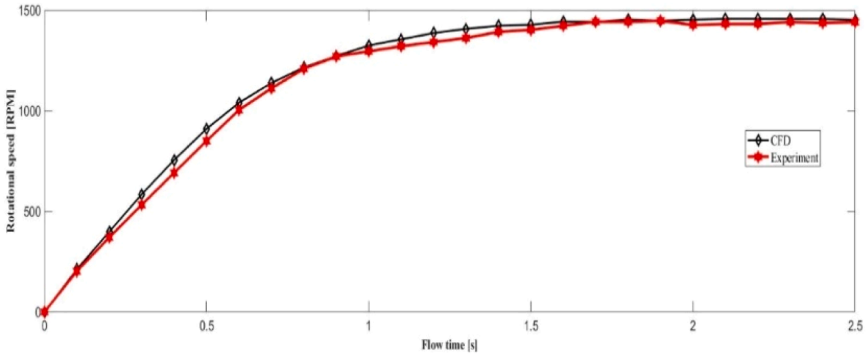

Fig. 8. The comparison of rotational speed of PAT using experimental and numerical methods.

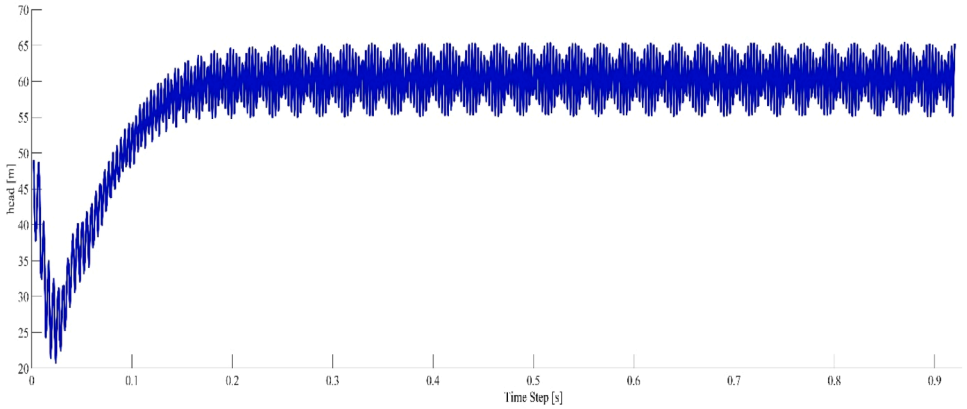

Fig. 9. The head variations in pump as turbine start-up.

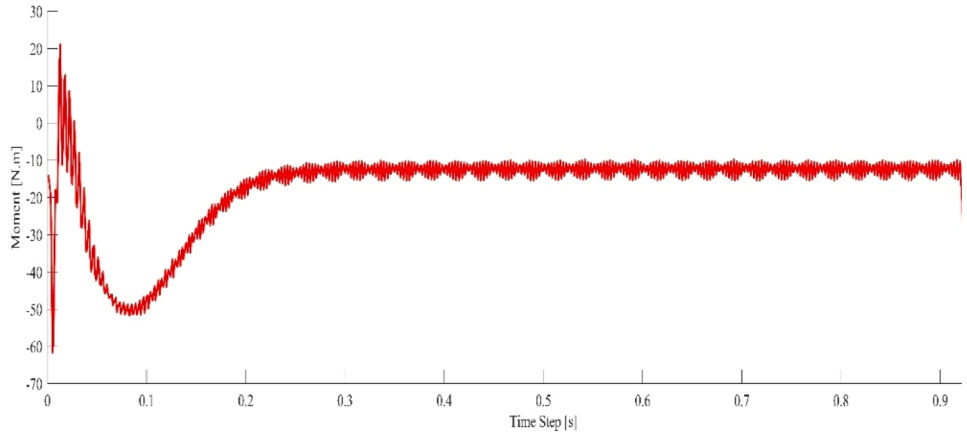

Fig. 10. During start-up, the pump's momentum varies as the turbine does.

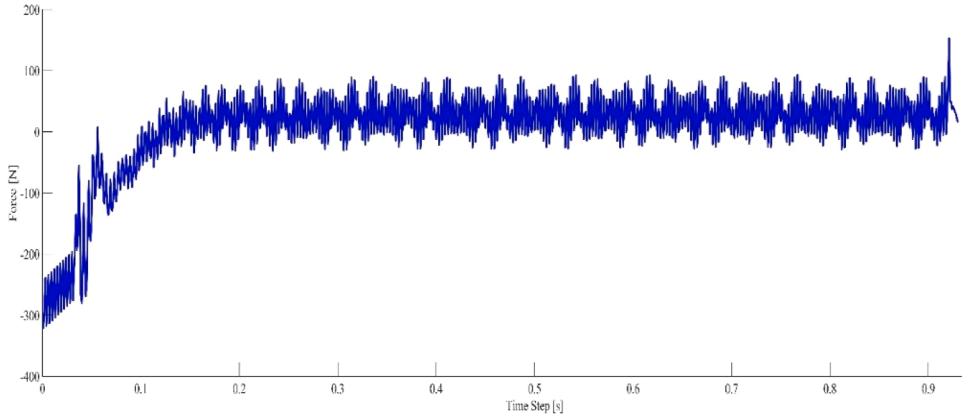

Fig. 11. The tangential force exerted on the blade variations in the pump acts as a turbine during the start-up phase.

response. Later on, the time interval between consecutive highs of the time domain curve steadily decreases as the amount of the pressure fluctuation drops quickly. In general, the magnitude of pressure fluctuations decreases throughout the startup process. The pressure variations were simulated for different steady-state velocities of 1450 RPM, 2900 RPM, and 4500 RPM. As shown in the figure, the pressure fluctuation range increases as the steady-state velocity increases while frequency decreases.

3.4. Internal flow analysis

The startup characteristics of a centrifugal pump operating as a turbine were concerned with how it behaves during the initial phase of operation when transitioning from a stationary state to reaching its full operational speed. A thorough understanding of these startup characteristics is essential to ensuring a smooth and efficient transition process. By considering the various factors that influence the startup, it becomes possible to optimize the pump design and ensure safe and reliable operation. The total pressure distributions of the PAT over time were

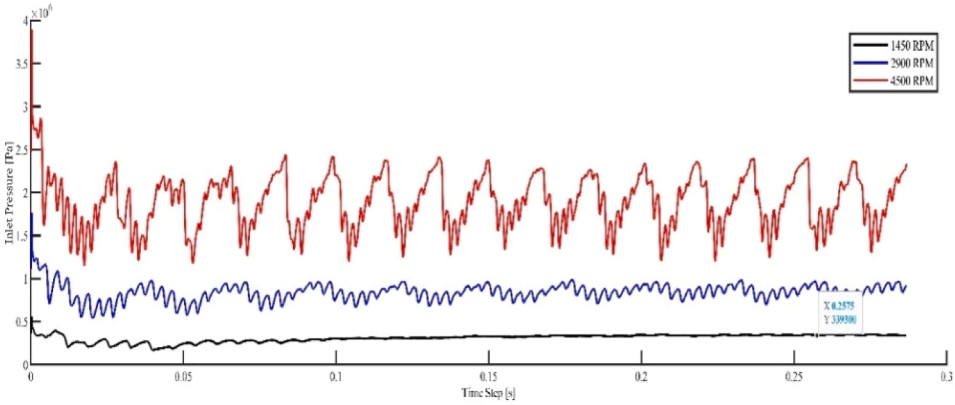

Fig. 12. The start-up pressure of PAT varies at various steady state velocities.

analyzed to discover the development of the internal flow field at start-up for a mass flow rate of 36 kg s^{-1} and speed of 4500 RPM. Fig. 13 depicts the instantaneous total pressure distributions in the vertical plane during the startup process. The figure reveals that the total pressure is high at the blade tip in all cases. Besides being higher at the initial phase and decreasing progressively, it reached a stabilized phase after 0.2 s. This implies that the impeller blades were exposed to severe instantaneous total pressure during the reverse flow and need special treatment to enhance their mechanical properties. In addition, a significant number of low-pressure areas over the impeller at $t = 0.5$ s decreases as the rotation speed increases, and the low-pressure area coverages in the impeller progressively decrease. After $t = 2$ s, the rotating speed has a tendency to be stable and attain the rated rotational speed; the pressure in the volute casing decreases progressively along the passage; and it has a gradient distribution in the impeller. The low-pressure areas also concentrate across the inner edge of the impeller.

The turbulent kinetic energy change through the vertical plane of the PAT over time was investigated to further understand the start-up process. Fig. 14 displays the turbulent kinetic energy distributions of the vertical plane during the transient startup phase. At $t = 0.5$ s, the figure reveals the formation of vast turbulent kinetic energy in the impeller's flow passages. It states that a transitory impact has the potential to significantly increase the load on the blade surface, as well as to initially create vibration and deformation of the blade. Initially, when the pump starts up, the flow velocity within the pump increases as the pump accelerates. This increase in flow velocity led to an increase in turbulent kinetic energy due to the higher flow rates. As the rotating speed increases, the turbulent kinetic energy intensity in the impeller decreases. Later As the PAT reaches its operational speed and stabilizes, reaching its lowest at $t = 2$ s, small turbulent kinetic energy continues to exist after $t = 2$ s, primarily focusing on the blade's tip face. This decrease occurs due to the establishment of a more stable flow pattern within the pump, which can reduce turbulence levels compared to the initial startup phase.

4. Conclusions and recommendations

The current paper used numerical simulation and experiments to study the PAT's flow field behaviors and startup characteristics. The conclusions drawn from the study results can be abridged aforementioned:

- When the system first started up, there were robust vortexes and several low-pressure zones over the impeller. Then, as the rotation speed increases, the pressure gradient distributes along the flow path, causing the vortexes to decrease quickly and concentrate on the non-working side of the blade.
- The pressure variation reaches its peak value at the initial phase of the startup period. As the speed increases, the pressure variation magnitude of the volute reduces rapidly, while it weakens gradually within the impeller. The frequency of pressure variations is consistent with the number of blades at each location during an impeller rotation cycle, and the number of fluctuations at each position is a function of both blade number and rotation frequency.
- When the pump starts up, there is a noticeable shift in the pressure distribution over the pump blades. The vortex regions progressively expand, reach the leading edges of the blade and the impeller passage, and then contract.

The present study has disclosed some key technical issues in the PAT

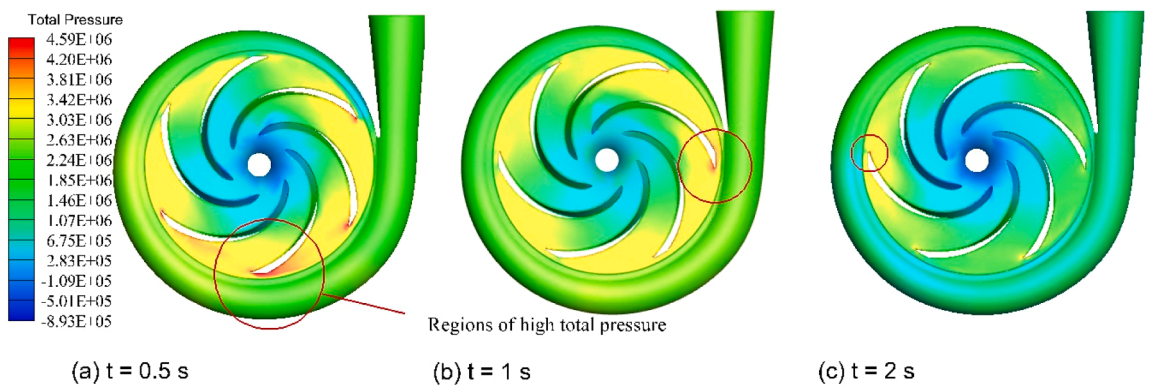

Fig. 13. Pressure distributions of PAT during the startup process: (a) $t = 0.5$ s; (b) $t = 1.5$ s; (c) $t = 2$ s.

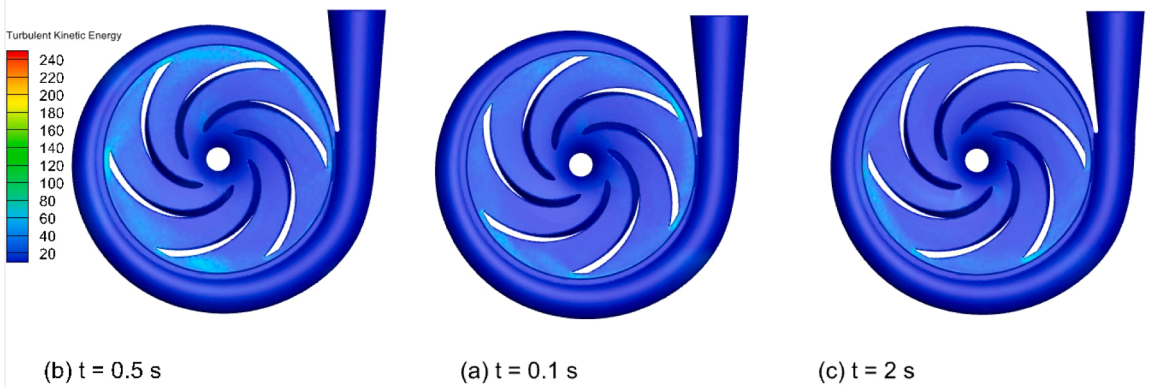

Fig. 14. Turbulent kinetic energy distributions of PAT at the startup: (a) $t = 0.5$ s; (b) $t = 1.5$ s; (c) $t = 2$ s.

startup process. However, issues like the fluid's compressibility during the pump startup remain unresolved and warrant consideration in future research.

CRediT authorship contribution statement

Dessie Tarekegn Bantelay: Writing – review & editing, Writing – original draft, Visualization, Validation, Software, Methodology, Investigation, Formal analysis, Data curation, Conceptualization. **Girma Gebresenbet:** Supervision, Methodology, Investigation. **Bimrew Tamrat Admasu:** Supervision, Methodology, Investigation. **Muluken Temesgen Tigabu:** Validation, Software, Methodology. **Muluken Zegey Getie:** Writing – review & editing, Visualization, Resources.

Declaration of competing interest

The authors declare that they have no known competing financial interests or personal relationships that could have appeared to influence the work reported in this paper.

Supplementary materials

Supplementary material associated with this article can be found, in the online version, at doi:10.1016/j.rineng.2025.103955.

Data availability

Data will be made available on request.

References

[1] D.T. Bantelay, et al., Analytical modeling of specific energy consumption and cost share in comprehensive textile industry: case study of Ethiopia, J. Optim. Ind. Eng. 13 (2) (2020) 47–56, https://doi.org/10.22094/JOIE.2019.580631.1612.
[2] D.T. Bantelay, et al., One-dimensional pump geometry prediction modeling for energy loss analysis of pumps working as turbines, Int. J. Thermofluids 21 (2024) 100562, https://doi.org/10.1016/j.ijft.2024.100562.
[3] D.T. Bantelay, G. Gebresenbet, B.T. Admassu, Challenges and prospects of hydro-pumps for small scale irrigation, in: Proceedings of the Advances of Science and Technology: 9th EAI International Conference, ICAST2021, Hybrid Event, Bahir Dar, Ethiopia, August 27–29, 2021, Springer, 2022. Proceedings, Part II.
[4] D.T. Bantelay, et al., Performance prediction of a pump as a turbine using energy loss analysis, Energy Rep. 12 (2024) 210–225, https://doi.org/10.1016/j.egyr.2024.06.023.
[5] Y.L. Zhang, Y.J. Zhao, Z.C. Zhu, A theoretical model for predicting the startup performance of pumps as turbines, Sci. Rep. 14 (1) (2024) 6963, https://doi.org/10.1038/s41598-024-57693-9.
[6] L. Zhou, et al., Application of entropy production theory for energy losses and other investigation in pumps and turbines: a review, Appl. Energy 318 (2022) 119211, https://doi.org/10.1016/j.apenergy.2022.119211.
[7] M. Liu, L. Tan, S. Cao, Performance prediction and geometry optimization for application of pump as turbine: a review, Front. Energy Res. 9 (2022) 818118, https://doi.org/10.3389/fenrg.2021.818118.
[8] L. Wang, et al., Geometrical optimization of pump-as-turbine (PAT) impellers for enhancing energy efficiency with 1-D theory, Energies 13 (16) (2020) 4120, https://doi.org/10.3390/en13164120 (Basel).
[9] D. Giosio, et al., Design and performance evaluation of a pump-as-turbine micro-hydro test facility with incorporated inlet flow control, Renew. Energy 78 (2015) 1–6, https://doi.org/10.1016/j.renene.2014.12.027.
[10] W. Li, et al., Study on the trajectory of tip leakage vortex and energy characteristics of mixed-flow pump under cavitation conditions, Ocean Eng. 267 (2023) 113225, https://doi.org/10.1155/2013/473512.
[11] K. Kan, et al., Pump as turbine cavitation performance for both conventional and reverse operating modes: a review, Renew. Sustain. Energy Rev. 168 (2022) 112786, https://doi.org/10.1016/j.rser.2022.112786.
[12] A.S. Dehkharqani, et al., A review of available methods for the assessment of fluid added mass, damping, and stiffness with an emphasis on hydraulic turbines, Appl. Mech. Rev. 70 (5) (2019), https://doi.org/10.1115/1.4042279.
[13] M. Amelio, S. Barbarelli, D. Schinello, Review of methods used for selecting pumps as turbines (PATs) and predicting their characteristic curves, Energies 13 (23) (2020) 6341, https://doi.org/10.3390/en13236341 (Basel).
[14] S.V. Jain, R.N. Patel, Investigations on pump running in turbine mode: a review of the state-of-the-art, Renew. Sustain. Energy Rev. 30 (2014) 841–868, https://doi.org/10.1016/j.rser.2013.11.030.
[15] M. Binama, et al., Investigation on pump as turbine (PAT) technical aspects for micro hydropower schemes: a state-of-the-art review, Renew. Sustain. Energy Rev. 79 (2017) 148–179, https://doi.org/10.1016/j.rser.2017.04.071.
[16] Y. Zhang, et al., Experimental study on a centrifugal pump with an open impeller during startup period, J. Therm. Sci. 22 (1) (2013) 1–6, https://doi.org/10.1007/s11630-013-0584-3.
[17] Y.L. Zhang, Y.J. Zhao, The atypical startup characteristics of a pump as turbine, Energy Sci. Eng. 10 (1) (2022) 132–144, https://doi.org/10.1002/ese3.1014.
[18] A.M. Malkawi, M.I. Alawneh, A. Bashaireh, A seamless start-up for a hybrid uninterruptible power supply based on a diesel generator and supercapacitor energy storage, Results Eng. (2024) 103418, https://doi.org/10.1016/j.rineng.2024.103418.
[19] D.T. Bantelay, Investigating water supply system electro-mechanical equipments problems: a case study of Ethiopia, J. Optim. Ind. Eng. 12 (2) (2019) 45–54, https://doi.org/10.22094/JOIE.2018.568034.1563.
[20] Z. Li, et al., Experimental and numerical study of transient flow in a centrifugal pump during startup, J. Mech. Sci. Technol. 25 (2011) 749–757, https://doi.org/10.3389/fenrg.2021.818118.
[21] Q. Li, et al., Study on the transient characteristics of the centrifugal pump during the startup period with assisted valve, Processes 8 (10) (2020) 1241, https://doi.org/10.3390/pr8101241.
[22] S. Fu, et al., Numerical simulation and experimental study of transient characteristics in an axial flow pump during start-up, Renew. Energy 146 (2020) 1879–1887, https://doi.org/10.1016/j.renene.2019.07.123.
[23] E. Casartelli, et al., CFD simulation of transient startup for a low specific-speed pump-turbine, in: Proceedings of the IOP Conference Series: Earth and Environmental Science, IOP Publishing, 2019, https://doi.org/10.1088/1755-1315/240/8/082007.
[24] T. Lei, et al., Role of blade rotational angle on energy performance and pressure fluctuation of a mixed-flow pump, Proc. Inst. Mech. Eng. A J. Power Energy 231 (3) (2017) 227–238, https://doi.org/10.1177/0957650917689948.
[25] C. Santolaria Morros, J.M. Fernández Oro, K.M. Argüelles Díaz, Numerical modelling and flow analysis of a centrifugal pump running as a turbine: unsteady flow structures and its effects on the global performance, Int. J. Numer. Methods Fluids 65 (5) (2011) 542–562, https://doi.org/10.1002/fld.2201.
[26] H. Tsukamoto, et al., Transient characteristics of a centrifugal pump during stopping period, J. Fluids Eng. 108 (4) (1986), https://doi.org/10.1115/1.3242594.
[27] Y.L. Zhang, et al., Experimental and theoretical study of a prototype centrifugal pump during startup period, Int. J. Turbo Jet-Engines 30 (2) (2013) 173–177, https://doi.org/10.1515/tjj-2013-0004.

[28] Y.L. Zhang, Y.J. Zhao, Atypical start-up experiments on pump as turbine, Adv. Mech. Eng. 13 (11) (2021) 16878140211062716, https://doi.org/10.1177/16878140211062716.
[29] Y.L. Zhang, et al., Effect of rotational speed and flowrate on the startup characteristics of a pumps as turbine, Meas. Control 55 (9–10) (2022) 1043–1056, https://doi.org/10.1177/00202940221098052.
[30] B. Chai, et al., Pressure fluctuation characteristics analysis of centrifugal pump as turbine in its start-up process, Actuators (2022), https://doi.org/10.3390/act11050132. MDPI.
[31] Y.L. Zhang, J.F. Li, Z.C. Zhu, The acceleration effect of pump as turbine system during starting period, Sci. Rep. 13 (1) (2023) 4913, https://doi.org/10.1038/s41598-023-31899-9.
[32] J. Cao, et al., Numerical theory and method on the modal behavior of a pump-turbine rotor system considering gyro-effect and added mass effect, J. Energy Storage 85 (2024) 111064, https://doi.org/10.1016/j.est.2024.111064.
[33] H. Gao, et al., Analysis of reactor coolant pump transient performance in primary coolant system during start-up period, Ann. Nucl. Energy 54 (2013) 202–208, https://doi.org/10.1016/j.anucene.2012.11.020.
[34] M.T. Tigabu, et al., Some effects of turbine inertia on the starting performance of vertical-axis hydrokinetic turbine, Ocean Eng. 252 (2022) 111143, https://doi.org/10.1016/j.oceaneng.2022.111143.
[35] U. Stuppioni, et al., Experimental and numerical characterization of the under-vane pressure in balanced vane pumps, Results Eng. 23 (2024) 102439, https://doi.org/10.1016/j.rineng.2024.102439.
[36] J. Hu, et al., Transient hydrodynamic behavior of a pump as turbine with varying rotating speed, Energies 16 (4) (2023) 2071, https://doi.org/10.3390/en16042071 (Basel).
[37] X. Bai, et al., Numerical investigation on the blade load distribution in a pump as turbine, Front. Energy Res. 11 (2023) 1220395, https://doi.org/10.3389/fenrg.2023.1220395.
[38] Y. Wei, et al., Numerical investigation of unsteady pressure pulsation characteristics in an ultra-low specific-speed centrifugal pump as a turbine, Front. Energy Res. 10 (2023) 1026886, https://doi.org/10.3389/fenrg.2022.1026886.
[39] D. Jianguo, et al., Computational analysis on numerical simulation of internal flow physics for pump as turbine in renewable small hydro energy generation, Complexity 2020 (1) (2020) 8869766, https://doi.org/10.1155/2020/8869766.
[40] T. Lin, et al., Application of enstrophy dissipation to analyze energy loss in a centrifugal pump as turbine, Renew. Energy 163 (2021) 41–55, https://doi.org/10.1016/j.renene.2020.08.109.
[41] J. Li, D. Meng, X. Qiao, Numerical investigation of flow field and energy loss in a centrifugal pump as turbine, Shock Vib. 2020 (2020) 1–12, https://doi.org/10.1155/2020/8884385.
[42] D. Štefan, et al., Study of the internal flow field in a pump-as-turbine (PaT): numerical investigation, overall performance prediction model and velocity vector analysis, Renew. Energy 156 (2020) 158–172, https://doi.org/10.1016/j.renene.2020.03.185.
[43] M. Rossi, A. Nigro, M. Renzi, Experimental and numerical assessment of a methodology for performance prediction of Pumps-as-Turbines (PaTs) operating in off-design conditions, Appl. Energy 248 (2019) 555–566, https://doi.org/10.1016/j.apenergy.2019.04.123.
[44] D. Adu, et al., Numerical investigation of transient vortices and turbulent flow behaviour in centrifugal pump operating in reverse mode as turbine, Mater. Sci. Energy Technol. 2 (2) (2019) 356–364, https://doi.org/10.1016/j.mset.2018.12.002.
[45] E. Frosina, D. Buono, A. Senatore, A performance prediction method for pumps as turbines (PAT) using a computational fluid dynamics (CFD) modeling approach, Energies 10 (1) (2017) 103, https://doi.org/10.3390/en10010103 (Basel).
[46] M. Pérez-Sánchez, et al., CFD analyses and experiments in a PAT modeling: pressure variation and system efficiency, Fluids 2 (4) (2017) 51, https://doi.org/10.3390/fluids2040051.
[47] S.S. Yang, S. Derakhshan, F.Y.J.R.E. Kong, Theoretical, numerical and experimental prediction of pump as turbine performance, Renew. Energy 48 (2012) 507–513, https://doi.org/10.1016/j.renene.2012.06.002.
[48] J. Fernández, et al., Numerical investigation of a centrifugal pump running in reverse mode, Proc. Inst. Mech. Eng. A J. Power Energy 224 (3) (2010) 373–381, https://doi.org/10.1243/09576509JPE757.
[49] F. Plua, et al., Analysis of applicability of cfd numerical studies applied to problem when pump working as turbine, Water 13 (15) (2021) 2134, https://doi.org/10.3390/w13152134 (Basel).
[50] M. Shamsuddin, N.M. Kamaruddin, Experimental study on the characterization of the self-starting capability of a single and double-stage Savonius turbine, Results Eng. 17 (2023) 100854, https://doi.org/10.1016/j.rineng.2022.100854.
[51] S.V. Patankar, D.B. Spalding, A calculation procedure for heat, mass and momentum transfer in three-dimensional parabolic flows, in Numerical prediction of flow, heat transfer, turbulence and combustion, Elsevier (1983) 54–73, https://doi.org/10.1016/B978-0-08-030937-8.50013-1.
[52] R.I. Issa, Solution of the implicitly discretised fluid flow equations by operator-splitting, J. Comput. Phys. 62 (1) (1986) 40–65, https://doi.org/10.1016/0021-9991(86)90099-9.
[53] H. Jasak, Z. Tukovic, Automatic mesh motion for the unstructured finite volume method, Trans. FAMENA 30 (2) (2006) 1–20.
[54] H. Jasak Dynamic mesh handling in OpenFOAM. in 47th AIAA aerospace sciences meeting including the new horizons forum and aerospace exposition. 2009.DOI: 10.2514/6.2009-341.
[55] J. Fahlbeck, et al., Performance characteristics of a contra-rotating pump-turbine in turbine and pump modes under cavitating flow conditions, Renew. Energy 237 (2024) 121605, https://doi.org/10.1016/j.renene.2024.121605.
[56] B.[Kim, et al., Investigation of a centrifugal pump for energy loss due to clearance thickness while pumping different viscosity oils, Results Eng. 18 (2023) 101038, https://doi.org/10.1016/j.rineng.2023.101038.